Simultaneous oil recovery and residual gas storage: a pore-level analysis using in-situ x-ray micro-tomography

S. Iglauer[1], A. Paluszny[2], M.J. Blunt[2]

[1]Curtin University, Department of Petroleum Engineering, 26 Dick Perry Avenue, 6151 Perth, Australia

[2]Imperial College London, Department of Earth Science and Engineering, Prince Consort Road, SW7 2AZ London, United Kingdom

Abstract

We imaged sandstone cores at residual gas saturation (S_{gr}) with synchrotron radiation at a nominal resolution of $(9\ \mu m)^3$. We studied two three-phase flooding sequences: 1. gas injection into a core containing oil and initial water followed by a waterflood (gw process); 2. gas injection into a waterflooded core followed by another waterflood (wgw process). In the gw flood we measured a significantly higher S_{gr} (= 20.6%; S_{gr} in the wgw flood was 5.3%) and a significantly lower residual oil saturation (S_{or}; S_{or} in the gw flood was 21.6% and S_{or} in the wgw flood was 29.3%). We also studied the size distribution of individual trapped clusters in the pore space. We found an approximately power-law distribution $N \propto s^{-\tau}$ with an exponent τ 2.02-2.03 for the residual oil clusters and $\tau = 2.04$ for the gas clusters in the gw flood. τ (= 2.32) estimated for the gas clusters in the wgw process was significantly different. Furthermore, we calculated the surface area A-volume V relationships for the clusters.

Again an approximate power-law relationship was observed, $A \propto V^p$ with p ≈ 0.75. Moreover, in the gw flood sequence we identified oil layers sandwiched between the gas and water phases; we did not identify such oil layers in the wgw flood. These results have several important implications for oil recovery, carbon geo-sequestration and contaminant transport: a) significantly more oil can be produced and much more gas can be stored using a gw flood; b) cluster size distributions for residual oil or gas clusters in three-phase flow are similar to those observed in analogue two-phase flow; c) there is a large cluster surface area available for dissolution of the residual phase into an aqueous phase; however, this surface area is significantly smaller than predicted by percolation theory (p ≈ 1), which implies that CO_2 dissolution trapping and contamination of aquifers by hazardous organic solvents is slower than expected because of reduced interfacial contact areas.

Keywords

Enhanced oil recovery, carbon geo-sequestration, residual oil, residual gas

1. Introduction

With a growing global population and fast economic development coupled with dwindling fossil fuel resources – and the fact that world energy consumption is currently mainly based on fossil fuels (they account for more than 80% of the total world's energy consumption [1]) - it is important to develop advanced technologies

that can recover additional fossil fuel. Another challenge concerns the carbon dioxide (CO_2) emissions associated with burning fossil fuels and the changes to global climate that may result. One technology to deal with this problem is CCS – Carbon Capture and Storage – where CO_2 is collected from fossil-fuel burning power stations and other industrial sites, transported and injected deep underground into saline aquifers of depleted oil and gas fields [2].

Crude oil is the most important fuel; in 2008 it contributed 41.6% (equivalent to an energy of 3505 Mtoe) to the world's total final consumption [1]. Crude oil, which is not produced by primary production or natural drive mechanisms such as solution gas drive, water influx or gravity drainage, can be produced by enhanced oil recovery (EOR) methods [3]. EOR processes include miscible or partially miscible gas flooding, thermal stimulation [3], surfactant flooding [4] or polymer flooding [5]. Gas injection EOR (GEOR, with natural gas, carbon dioxide CO_2, or nitrogen) is usually employed to displace and recover residual oil that remains in the reservoir after natural depletion and waterflooding.

In a GEOR process three fluid phases flow: oil, gas and brine; three-phase flow also occurs in carbon geo-sequestration (CCS) in depleted oil or gas reservoirs [6,7]. CCS can be combined with GEOR. The objective is to simultaneously maximize CO_2 storage and hydrocarbon recovery [8]. Gas is injected either as a secondary process, into oil and initial water, or as a tertiary process into residual oil and water after waterflooding. For carbon dioxide storage it is valuable to trap the CO_2 as a residual phase, and so both gas injection sequences can be followed by further waterflooding. We will compare these two processes in this paper.

Several researchers have investigated three-phase flow at the meso (centimetre) scale, mainly with the focus on oil recovery [9,10], fluid distributions [11], relative permeability [12-15], or capillary pressure measurements [16]. Pore-scale displacement studies have also been conducted [10,17-23]. These pore-scale studies employed 2D models, which are, however, not necessarily representative of reservoir flow conditions as the connectivity of the pore network cannot be captured correctly (for example the percolation threshold for 3D lattices is significantly lower than for 2D lattices [24]). In addition such 2D models typically use strongly simplified artificial materials – not reservoir rock – which may not be representative of reservoir conditions. Furthermore, three-phase trapping has been measured in rock samples [25-27], which is important for CCS risk and capacity assessments and related residual trapping capacity predictions [28].

To optimize GEOR, reservoir flow models are required that can predict the efficiency of oil recovery and associated time scales. However, because of the complexities of rock pore morphology, fluid-fluid and fluid-solid interactions, theoretical understanding is currently limited to simple models which only have limited predictive capabilities with scant physical foundation, based on pore-scale displacement processes. To overcome this, we analyse three-phase flow (oil, brine, gas) in a sandstone at the pore-scale (micrometre scale) in 3D with micro-computed tomography (μ-CT), and we compare two GEOR flooding sequences.

2. Experimental Methodology

We compared two GEOR flooding sequences:

(1) gas flood of a virgin oil reservoir; gas was directly injected into a core at connate water saturation (S_{wc}) followed by a chase brine injection (gw sequence), and

(2) gas flood of a waterflooded oil reservoir; where gas was injected into a waterflooded core at residual oil saturation (S_{or}) followed by chase brine injection (wgw sequence).

For these experiments we selected a clean, well-sorted relatively homogenous sandstone outcrop (Clashach, a quarried sandstone from Elgin in Scotland). The brine permeability was measured to be 8 x 10^{-14} m^2 (80 mD) [29] and porosity was 11.1%±0.5%. Clashach consists mainly of quartz (≥ 96wt%) with small amounts of K-feldspar, calcite and ankerite [30]. Oil (1-Bromododecane, purity ≥ 99.5 mass%, supplied by Aldrich), gas (N_2, purity >99.998 mass%) and brine (10wt% potassium iodide (KI) in deionized water) were selected as fluid phases. The brine was doped with KI and the special brominated oil was used to guarantee sufficient CT contrast. The fluid-fluid interfacial tensions are listed in Table 1. We assume that the rock is water-wet.

The spreading coefficient is defined by:

$$S = \gamma_{gw} - \gamma_{ow} - \gamma_{go} \quad (1)$$

where γ_{gw} is the gas-brine interfacial tension, γ_{ow} is the oil-brine interfacial tension and γ_{go} is the gas-oil interfacial tension. The spreading coefficient S has a value of -11.05 mN/m. All experiments were conducted at ambient laboratory conditions, that is 293K and 0.1MPa. A small cylindrical core plug of 5mm diameter and 10mm length was drilled and placed into a fluoroplastic heatshrink sleeve. Both plug ends were sealed with standard stainless steel Swagelok fittings, and this core system was heated so that the heatshrink sleeve strongly adhered to the plug and fluid by-passing was prevented. The fluids were injected with standard syringe pumps (Teledyne ISCO, model 500D, Lincoln, NE, USA) into the plug positioned horizontally.

Table 1

Interfacial tensions of the fluids used.

fluid-fluid system	interfacial tension [mN/m]
water/1-bromododecane*	γ_{ow} = 52.09
water/nitrogen**	γ_{gw} = 72
1-bromododecane/nitrogen***	γ_{go} = 30.96

*measured at 295K [31].

**measured at 293.15K and 0.101 MPa [32].

***surface tension of 1-bromododecane.

For both flood sequences, the cores were first completely saturated with brine under vacuum and then approximately 20 pore volumes (PV) of oil were injected at a low capillary number ($\mu q/\gamma \approx 5 \times 10^{-6}$, where q is the Darcy flow rate, μ is the viscosity of

the injected phase and γ is the interfacial tension), which is representative of flow conditions in a reservoir. After injection of a few PV of oil, water production ceased. This represents a virgin oil reservoir where oil displaced most of the formation water over geological times except the immobile (connate) water S_{wc}. S_{wc} was the starting point for both flooding sequences. For the gw flood the next step was to inject approximately 200 PV of gas at a capillary number of approximately 10^{-5} until liquid production by viscous displacement ceased (visual observation). Then approximately 20 PV of chase brine were injected at a low capillary number (10^{-6}) until no oil or gas was produced and the residual gas saturation S_{gr} was reached. In case of the wgw sequence, the core at S_{wc} was first waterflooded with approximately 20 PV of brine at a low capillary number (10^{-6}) to S_{or}, and then gas and chase brine were injected using the same procedure as in the gw process. During flooding, the cores were held horizontally. Bond numbers were estimated to be $\approx 10^{-5}$ for the liquid-gas system and 10^{-7} for the oil-brine system; we therefore do not expect the residual clusters/residual saturations to be influenced by buoyancy forces [33].

Both specimens were then scanned with synchrotron radiation at the SYRMEP beamline of the Elettra light source facility in Trieste, Italy (photon energy = 30 keV). We analyzed a subvolume of the resulting images consisting of 300^3 voxels (19.683 mm^3, nominal voxel resolution of 9 μm).

All raw μ-CT images were cleaned of ring artefacts by applying a stripe removal algorithm based on combined wavelet—Fourier filtering [34]. Salt-and-pepper noise was removed using a conservative anisotropic regularization filter [35]. The phases were then segmented according to their CT contrast using multi-thresholding, i.e. by identifying peaks in the gray-level histogram of each image based on Otsu's algorithm

[36]. Figure 1 shows slices through the rock and fluid phase distributions for both flood sequences, and Figure 2 displays observed residual oil and gas clusters in 3D.

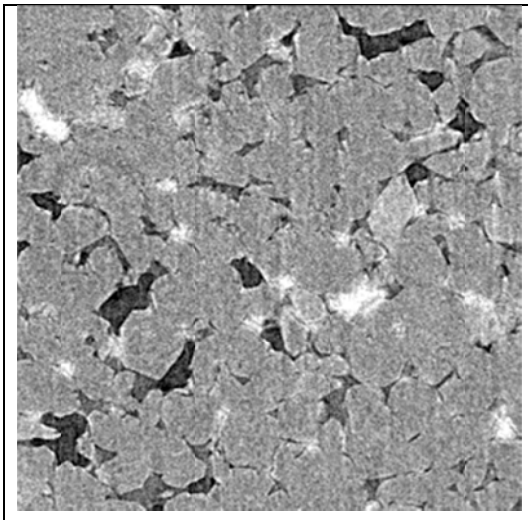

(a) gw flood.

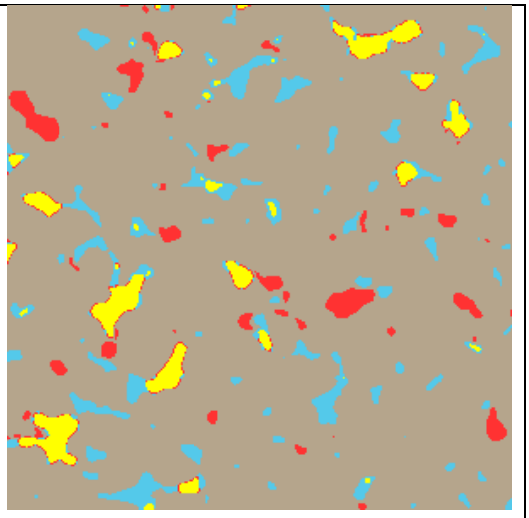

(b) gw flood.

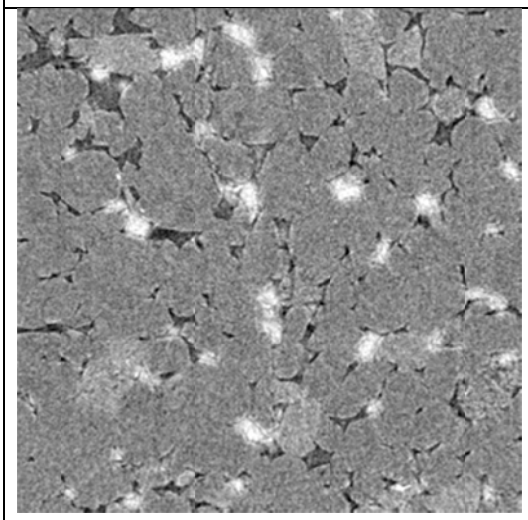

(c) wgw flood.

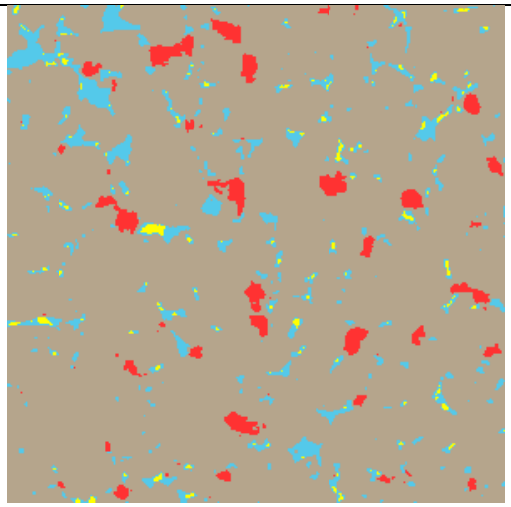

(d) wgw flood.

Figure 1: 2D image slices through the rock and fluids at residual gas saturation after chase brine injection. (a) gw flood sequence, raw image: oil is white, gas is black, brine dark grey and sandstone is light grey. (b) gw flood sequence: segmented images, brine is light blue, oil is red, gas is yellow and rock is brown. (c) wgw flood sequence, raw image: oil is white, gas is black, brine dark grey and sandstone is light grey. (d)

wgw flood sequence: segmented images, brine is light blue, oil is red, gas is yellow and rock is brown. All images show an area of 2.7 mm x 2.7 mm = 7.29 mm^2.

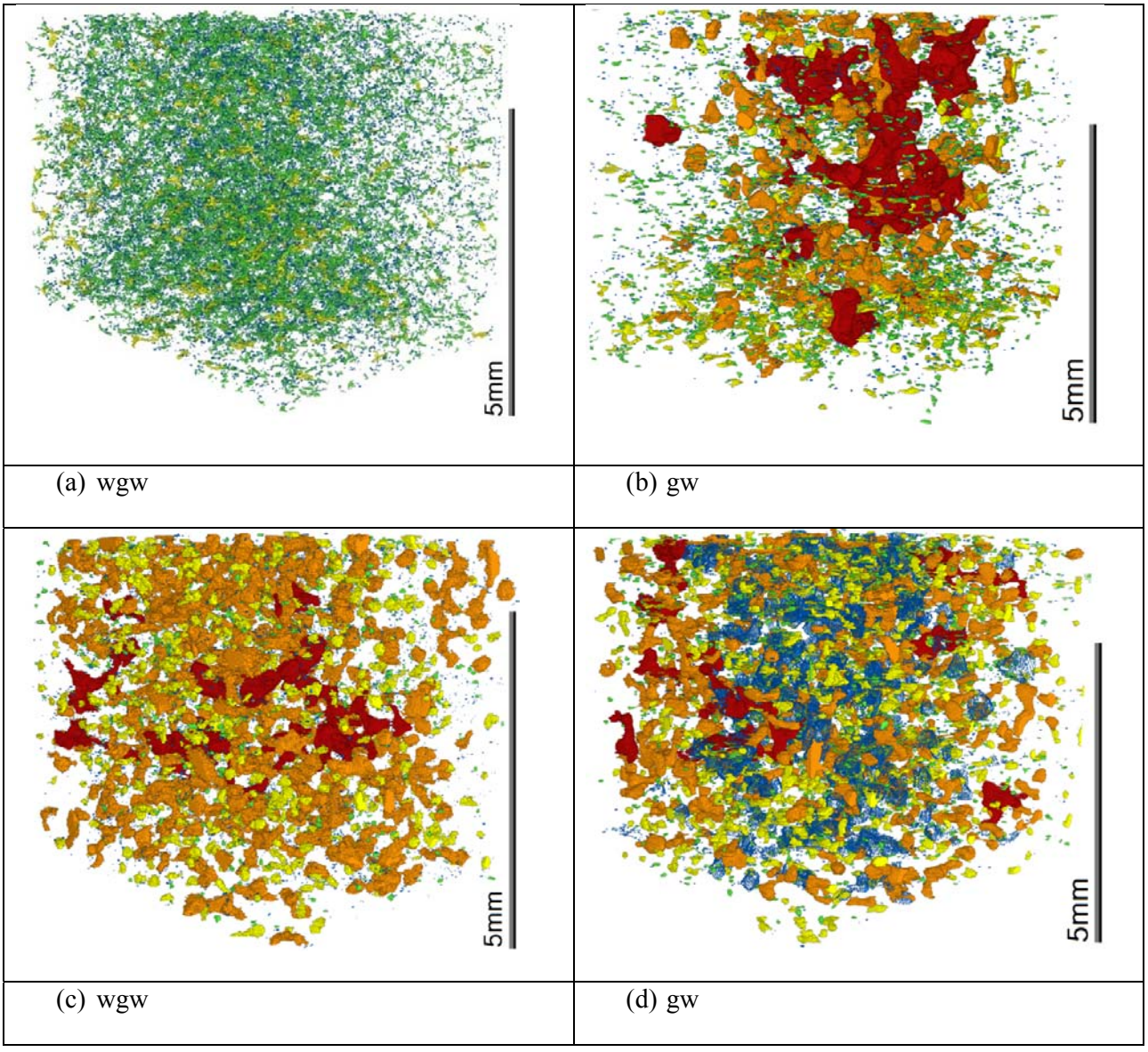

(a) wgw (b) gw

(c) wgw (d) gw

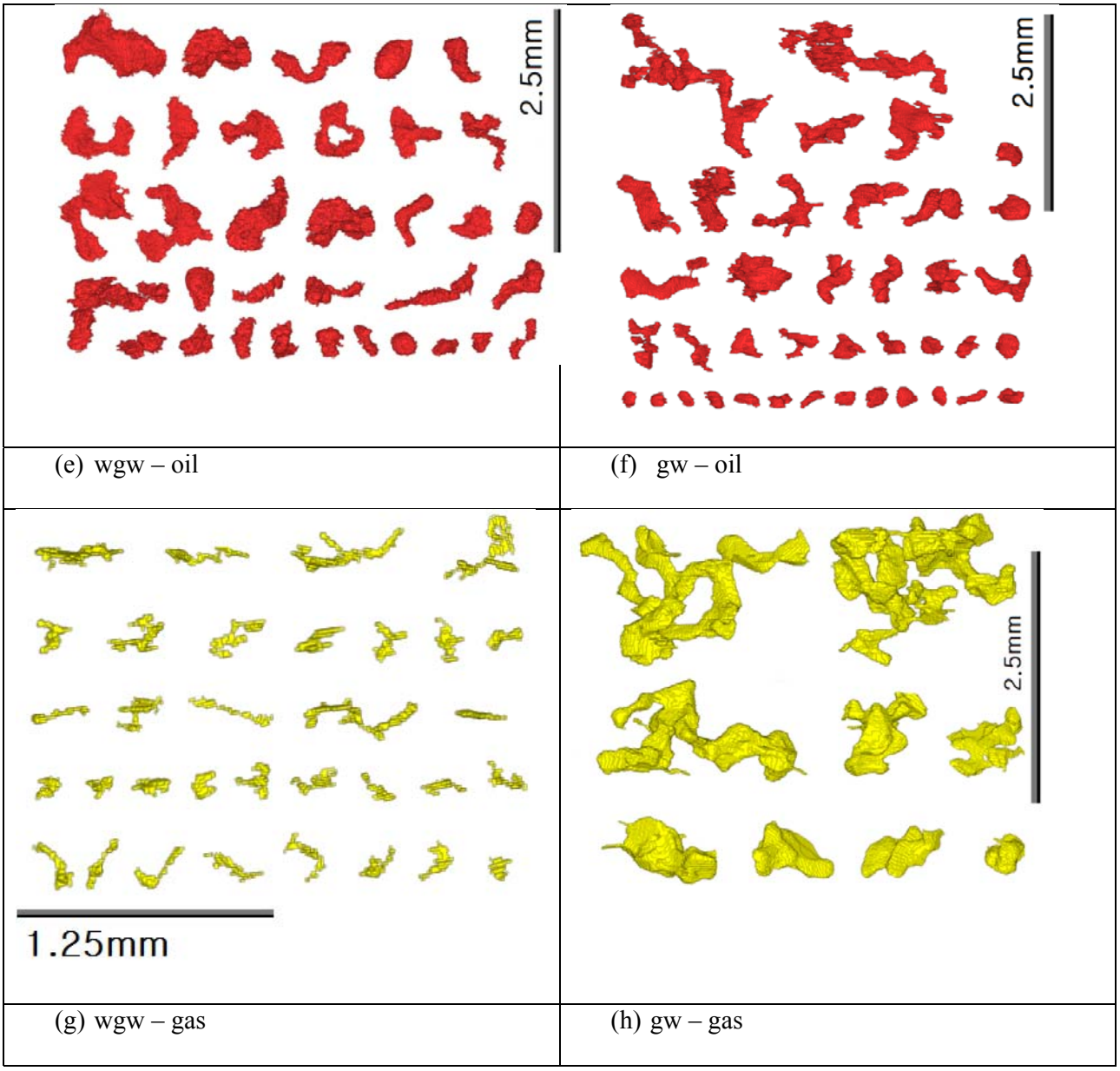

(e) wgw – oil

(f) gw – oil

(g) wgw – gas

(h) gw – gas

Figure 2: 3D images of residual oil and gas clusters (rock and brine phases were cropped out). (a) residual gas clusters in the wgw flood. (b) residual gas clusters in the gw flood. (c) residual oil clusters in the wgw flood. (d) residual oil clusters in the gw flood. (a)-(d): All volumes displayed are 2.7 mm x 2.7 mm x 2.7 mm = 19.683 mm^3. The clusters are coloured according to size: blue < 235 nl (nanolitre) (1000 voxels), green 235-2350 nl (1000-10000 voxels), yellow 2350-23500 nl (10000-100000 voxels), orange 23500-235000 nl (10^5–10^6), red > 235000 nl (>10^6 voxels). (e) wgw flood: selected individual residual oil clusters: the largest clusters (6250-13000 nl;

26564-54797 voxels), several medium-sized clusters (1200-2350 nl, 5000-10000 voxels) and some small clusters (2.35-235 nl, i.e. 10-1000 voxels) are shown. (f) gw flood: selected individual residual oil clusters: the largest clusters (3800-6900 nl, 16180-29251 voxels), several medium-sized clusters (1200-2350 nl, 5000-10000 voxels) and some small clusters (2,35-235 nl, 10-1000 voxels) are shown. (g) wgw flood: selected individual residual gas clusters: the largest clusters (75-100 nl, 319-434 voxels), several medium-sized clusters (23.5-26 nl, 100-110 voxels) and some small clusters (11.7-16.5 nl, 50-70 voxels) are shown. (h) gw flood: selected individual residual gas clusters: the largest clusters (7400-11000 nl, 31393-46222 voxels), several medium-sized clusters (1200-2350 nl, 5000-10000 voxels) and some small clusters (2.35-235 nl, 10-1000 voxels) are shown.

3. Results and Discussion

3.1 Fluid saturations – residual oil and gas saturations

Fluid phase saturations measured from the μ-CT images are listed in Table 2 for both flooding sequences. In addition several meso-scale literature values are added for comparison. It is clear from our datasets that much more gas can be stored and more incremental oil can be produced if gas is directly injected into a virgin oil reservoir (gw flood sequence).

Furthermore, we have previously studied similar two-phase (brine and oil) flow processes at the micro- and meso-scale [30,37-39]. From the comparison of these datasets we reach several conclusions:

1. More oil can be recovered by three-phase flow, i.e. a lower S_{or} can be achieved, when gas injection is employed compared to water injection alone.
2. If rock wettability changes from water-wet (in these experiments) to more oil-wet conditions, then this significantly influences oil recovery [30].
3. The rock pore morphology and porosity significantly influence S_{or} [28].

Table 2

Measured phase saturations for the two flood sequences representing a GEOR in a virgin oil reservoir (gw) and a waterflooded oil reservoir (wgw). S_{or}^{3p} is the three-phase residual oil saturation, S_{w}^{3p} is the three-phase residual water saturation and S_{gr}^{3p} is the three-phase residual gas saturation (after the final waterflood). Three-phase and two-phase micro- and meso-scale literature datasets are added for comparison.

Experiment	flood sequence	porous medium	porosity	permeability [m^2]	residual oil saturation S_{or}^{3p*}	water saturation S_{w}^{3p}	residual gas saturation S_{gr}^{3p}
Three-phase our result	gw	Clashach sandstone (water-wet)	0.116	8×10^{-14}**	0.216	0.578	0.206

Three-phase our result	wgw	Clashach sandstone (water-wet)	0.107	8 x 10^{-14**}	0.293	0.654	0.053
Three-phase [25]	gw	quartz sand pack (water-wet)	0.37	3.16 x 10^{-11}	0.10	0.68	0.22
Three-phase [26]	gw	Estaillades limestone	0.23	2.12 x 10^{-13}	0.20	0.60	0.20
Three-phase [27]	gw	Aerolith (artificial material)	0.39	5.72 x 10^{-12}	0.18	0.68	0.14
Two-phase [37]	w	Clashach sandstone (water-wet)	0.111	8 x 10^{-14**}	0.352	0.648	0
Two-phase [30]	w	Clashach sandstone (oil-wet)	0.144	8 x 10^{-14**}	0.188	0.812	0
Two-phase [40]	w	quartz sand pack (water-wet)	0.370	3.16 x 10^{-11}	0.128	0.872	0

*Two-phase S_{or} for the two-phase experiments.

**[29]

**w stands for the two-phase waterflood sequence: waterflooding a core containing oil and connate water with no gas injection.

Fayers [41] suggested that the residual oil saturation in three-phase flow systems is reduced compared to equivalent two-phase systems:

$$S_{or}^{3p} = S_{or}^{2p} - aS_{gr}^{3p} \quad (2)$$

where S_{or}^{3p} is the three-phase residual oil saturation, S_{or}^{2p} is the two-phase residual oil saturation (S_{or}^{2p} = 35% was measured in a separate study on the same rock system [37]), S_{gr}^{3p} is the three-phase residual gas saturation, and *a* is a fitting coefficient. We find *a* = 0.65 for the gw flood, which is close to the previous literature value (*a* = 0.55, [41]) and lies within the range mentioned in the literature (0.2-1). For the wgw sequence we observed a different coefficient *a* (= 1.07 which is slightly above the maximum value cited in the literature), so clearly the flooding history is a major factor influencing the coefficient *a*.

3.2 Residual oil and gas cluster size distributions

We proceeded with analysing the residual oil and gas cluster size distributions for both flood sequences and plotted them in Figure 3 (gw sequence) and Figure 4 (wgw sequence). n(s) is the normalized number of residual clusters of size s (s is given in voxels), $n(s) = N(s)/N_v$, where N(s) is the number of residual clusters of size s counted and N_v is the total number of pore space voxels. In addition, we plotted the

cumulative cluster size distribution S (S(1) is the residual oil or residual gas saturation) as suggested by Dias and Wilkinson [42], S represents the contribution of clusters larger than size s to the residual saturation; $S(s) = \sum_{s}^{\infty} s \cdot n(s) \propto s^{-\tau+2}$.

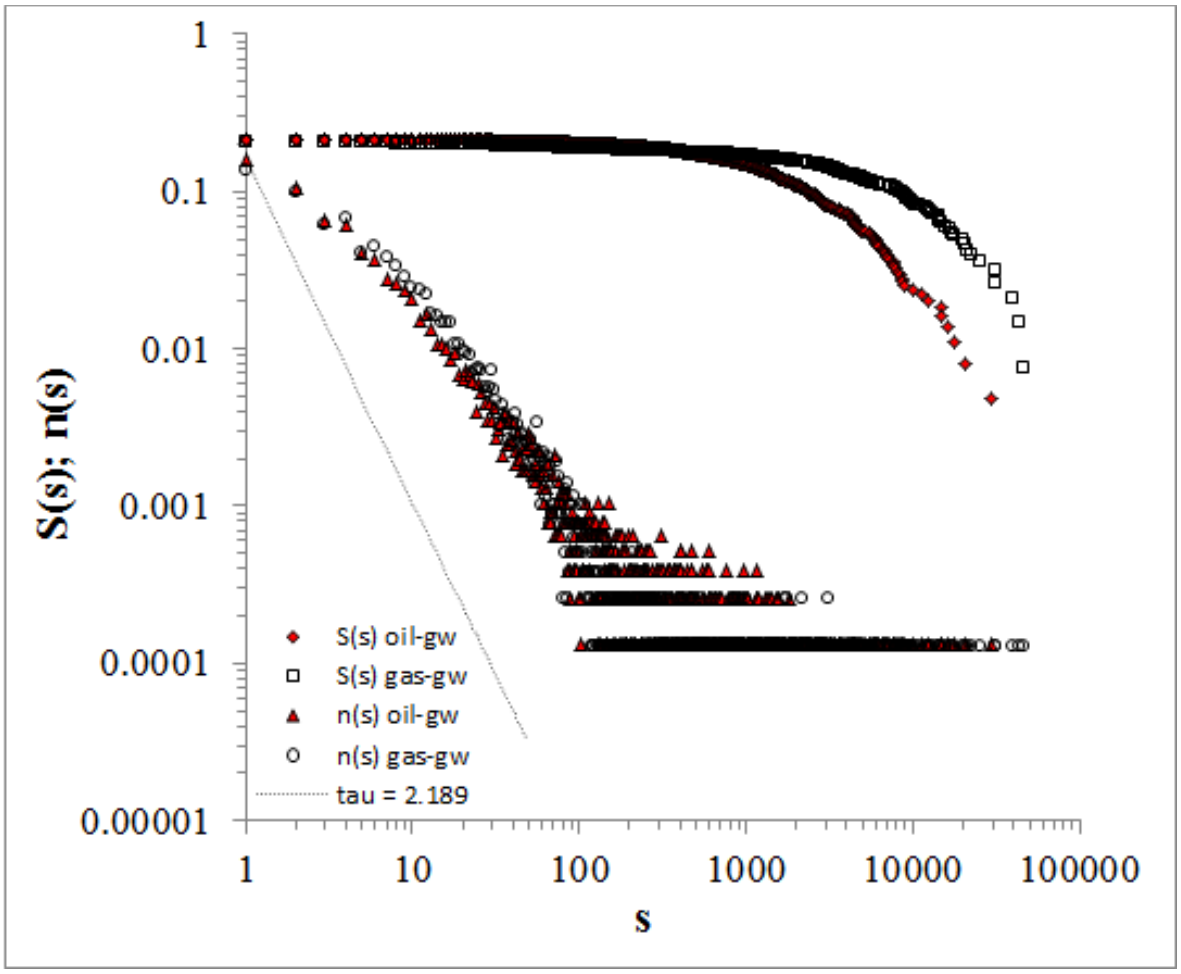

Figure 3: Residual oil and gas cluster size distributions for the gw flood sequence; S(s) is the cumulative normalized distribution and n(s) is the normalized distribution. S(1) is the residual phase saturation. The dashed line indicates an oil cluster distribution with $\tau = 2.189$, as theoretically predicted by percolation theory [44].

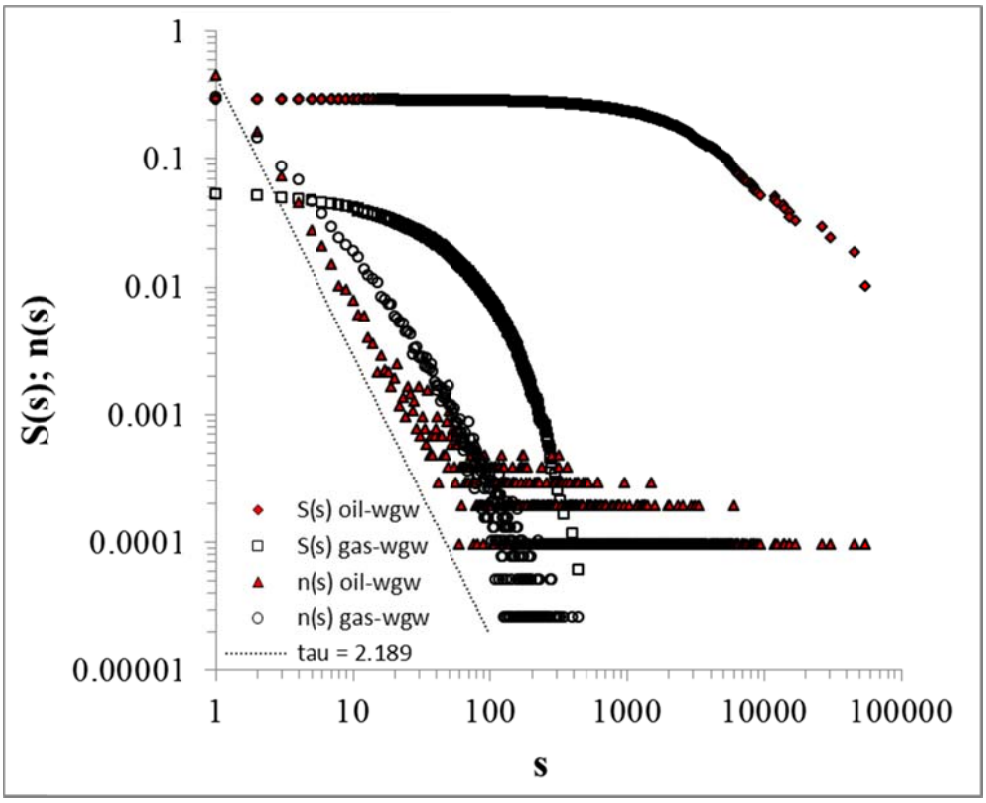

Figure 4: Residual oil and gas cluster size distributions for the wgw flood sequence; S(s) is the cumulative normalized distribution and n(s) is the normalized distribution. S(1) is the residual phase saturation. The dashed line indicates an oil cluster distribution with $\tau = 2.189$, as theoretically predicted by percolation theory [44].

We then considered percolation theory, which states that the cluster size distribution follows a power-law according to $N(s) \sim s^{-\tau}$ [43] where τ is equal to 2.189 [44]. We estimated τ from the cumulative curves as suggested by Dias and Wilkinson [43]. Results for τ, obtained with best fits through the linear parts of the S distributions, are shown in Table 3, together with additional literature data.

Table 3

Residual cluster size distribution power-law exponents τ estimated for various flood sequences (compare text for details). 2p stands for two-phase and 3p for three-phase. In addition, the area A-volume V correlation exponent p (assuming $A \propto V^p$) is shown for the experimental and some ideal systems.

System	τ	p
2p-Clashach[*]	2.05	0.7488
2p-Doddington[*]	2.05	0.7566
2p-Clashach (oil-wet)[**]	2.12	0.7702
3p-gw-oil	2.03	0.7289
3p-gw-gas	2.04	0.7297
3p-wgw-oil	2.02	0.7284
3p-wgw-gas	2.32	0.7757
2p-glass beads[***]		0.84
ideal sphere		2/3
percolation theory	2.189[****]	1[*****]

[*][37]

[**][30]

[***][45]

[****][44] – these values were derived by Monte Carlo simulations.

*****[25]

The oil cluster size distributions are similar for both three-phase flood sequences, although the wgw flood had a few larger oil clusters (largest oil cluster was 54797 voxels = 0.039947 mm^3) than the gw flood (largest cluster was 29251 voxels = 0.021324 mm^3), but fewer medium-sized clusters, so that overall a lower S_{or} was measured for the gw flood (21.6%) than for the wgw flood (S_{or} = 29.3%). The τ value estimated for the gw flood (=2.03) was very similar to the τ value estimated for the wgw flood (= 2.02); these cluster size distribution exponents for the three-phase floods can be compared with analogue τ values for two-phase floods (w flood sequence), for which τ = 2.05 was identified [37]. A smaller τ indicates that there are relatively fewer small clusters and more large clusters.

The τ value estimated for the residual gas cluster size distribution in the gw flood is also similar (= 2.04); however τ estimated for the residual gas cluster size distribution in the wgw flood is significantly different (τ = 2.32). This difference in residual gas cluster size distributions (gw versus the wgw flood sequences) is also reflected in the significantly higher S_{gr} (20.5%) in the gw flood than in the wgw flood (S_{gr} = 5.3%); and many more larger gas clusters were counted in the gw flood. The largest gas cluster in the gw flood had a volume of 46222 voxels (= 0.033696 mm^3) while the largest gas cluster in the wgw flood had a volume of only 434 voxels (= 0.000316 mm^3).

Moreover, we note here that wettability can also play a role in terms of τ, for a weakly oil-wet system (two-phase, oil/brine, Amott-Harvey index = -0.1), a τ = 2.12 was estimated [30] and for a supercritical CO_2-brine-sandstone outcrop a τ = 2.01 was estimated [46]. This indicates that a $scCO_2$/brine/sandstone system is not strongly water-wet, and more likely weakly water-wet or mixed-wet, with important implications for residual and structural trapping, and consistent with meso-scale measurements for residual trapping [47], a capillary pressure measurement [48], relative permeability measurements [49], fluid distributions in 2D micromodels [50], and direct contact angle measurements [51-54] and molecular dynamics computations [55,56].

Furthermore, the flood sequence can have an impact on the morphology of the residual clusters: the residual gas clusters in the gw flood are large and bulky, it appears that they resemble the connected pore space of the largest pores; while the residual gas clusters in the wgw flood are much thinner and smaller, which implies different displacement and snap-off processes. A similar, but less extreme scenario, was observed for the residual oil clusters, although this time the more ramified clusters (the oil clusters were of similar size for both flood sequences) were measured in the gw flood. This implies that in the wgw flood, where oil is already trapped in disconnected clusters (after the first waterflood, compare Iglauer et al. [37] for a detailed analysis) and surrounded by brine – before the gas flood starts, a) oil is subject to much less mobilization by gas and the subsequent waterflood (compare S_{or}^{3p} = 0.293 for the wgw flood with S_{or}^{3p} = 0.216 for the gw flood), oil is inhibited from mobilization by the surrounding water, and b) the gas changes the residual cluster shape only marginally, while in the gw flood gas directly displaces oil, inducing a

stronger change in the oil clusters' morphology. This direct displacement is also more efficient in terms of oil production. This is discussed further in section 3.5.

3.3 Oil layers

We identified oil layers in the gw flood (cp. Figures 1 and 5). These layers were fairly thick, several micrometres on average, and they surrounded gas clusters fully or partially. To be precise, our definition of oil layers in this paper is a thin oil structure of thickness 1-2 voxels with a significant 2D extension. However, we cannot observe thinner oil layers although they most likely exist as demonstrated in 2D micromodel experiments [17].

Oil layers form because gas is the non-wetting phase, and water the wetting phase in the system we studied. Oil is the intermediate-wet phase and spreads between gas and water due to intermolecular forces [53]. We did not observe such oil layers in the wgw flood; again, this is probably due to the limited resolution of the μ-CT images – we conclude that the oil layers are thinner than around 10 μm in this case. It is likely that these oil layers were disconnected oil lenses as the system is non-spreading; this is discussed further later.

Furthermore, although the images show that oil layers in several pores directly touch the rock surface, our interpretation is that the image resolution is insufficient to detect the very thin water layer between the oil and the rock, which however most likely exists as the rock is water-wet (i.e. the thickness of this water layer is below the voxel resolution of the scan).

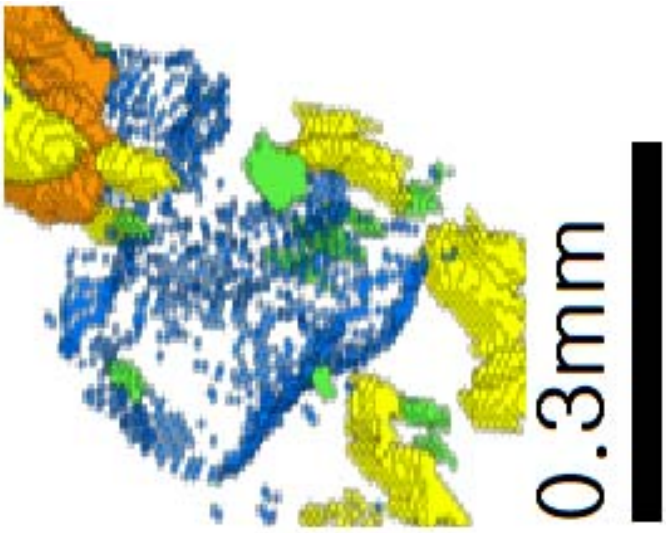

Figure 5: Oil layer (blue) in the gw flood. The orange, green and yellow volumes are oil droplets.

3.4 Residual oil and gas cluster surface quantification

We then determined the surface area of each residual oil and gas cluster and plotted the surface area of each cluster against its volume (Figures 6-9).

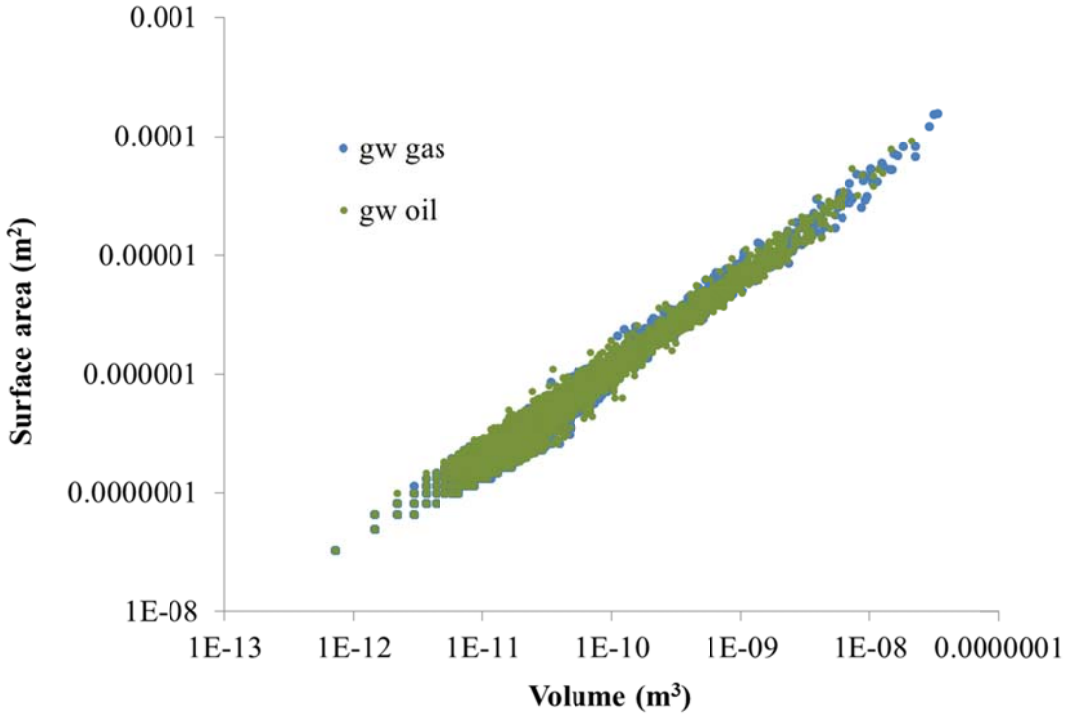

Figure 6: Residual oil and gas cluster surface areas for the gw flood sequence plotted against cluster volume.

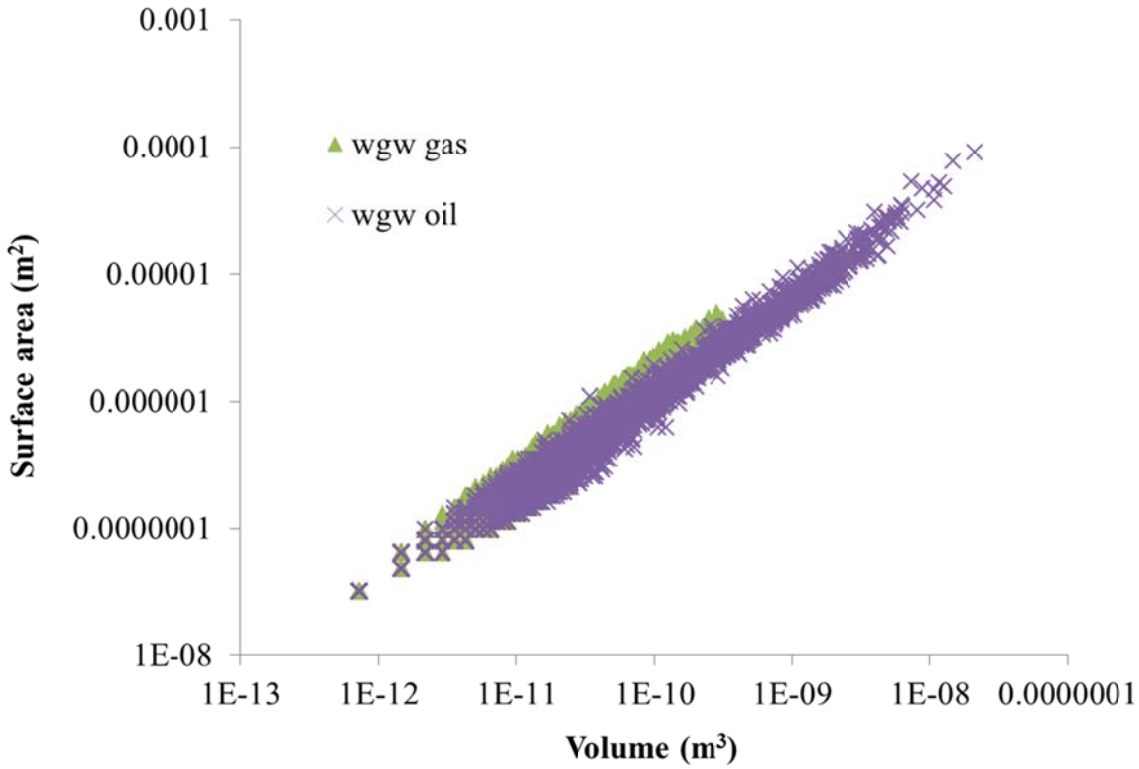

Figure 7: Residual oil and gas cluster surface areas for the wgw flood sequence plotted against cluster volume.

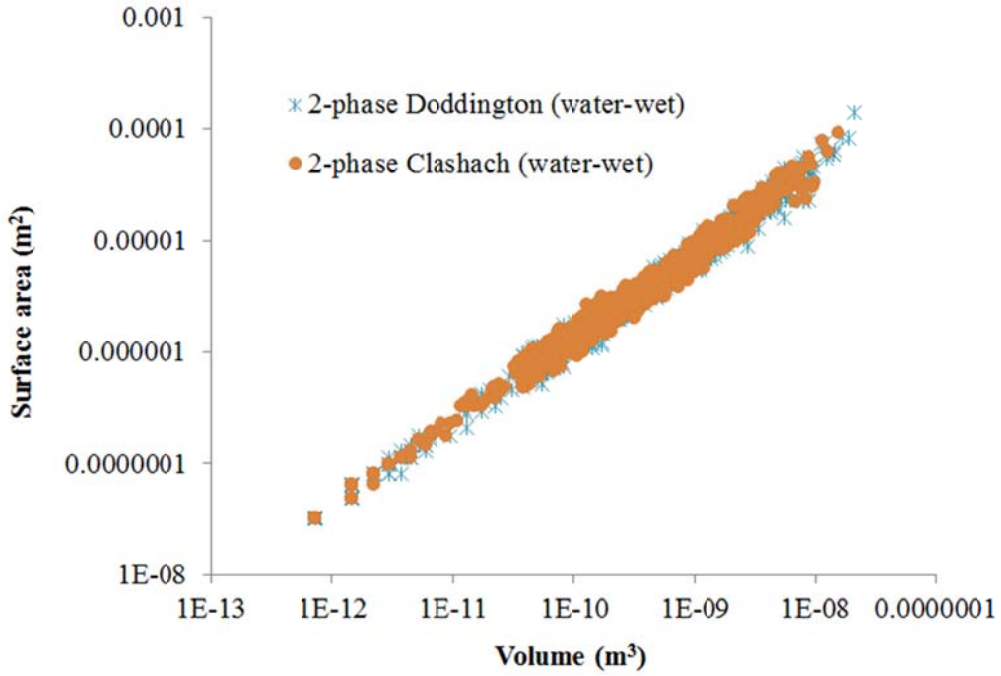

Figure 8: Residual oil cluster surface areas for brine-oil two-phase flow (water-wet sandstone [37]).

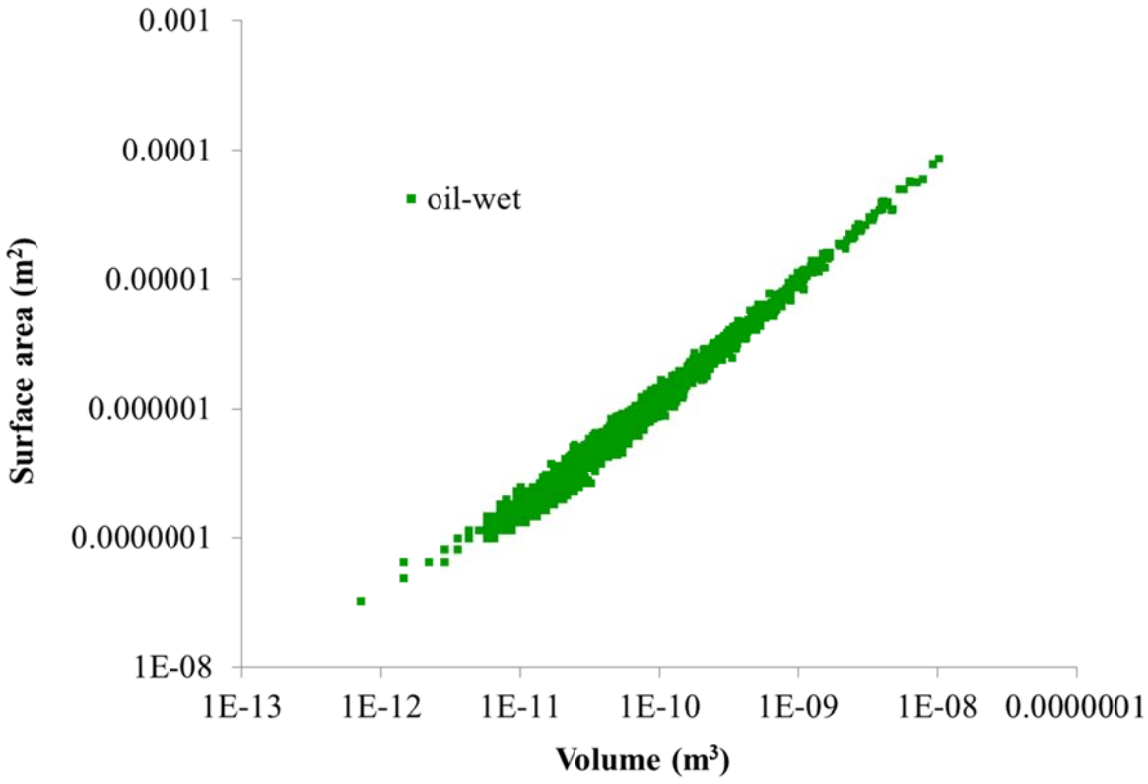

Figure 9: Residual oil cluster surface areas for brine-oil two-phase flow (oil-wet sandstone [30]).

From these datasets we estimated the surface area-volume power-law correlation exponent p for each system, assuming that $A \propto V^p$, following Landry et al. [45]. A is the cluster surface area and V the cluster volume. Our results are listed in Table 3, and they are consistent with Landry et al.'s [45] result. Based on these experimental datasets we conclude that p (≈ 0.75) is smaller than expected from percolation theory, which finds p ≈ 1 [25]. This means that the residual clusters are more compact than predicted by percolation theory. This has important implications for carbon geo-sequestration and contaminant transport: dissolution of the residual organic phase or

CO_2 phase into the aqueous phase is slower than predicted by percolation theory as the surface area/volume ratio for each cluster is smaller, leading to slower mass transfer rates [57].

3.5 Discussion

In this study we only consider microscopic sweep efficiency at the pore-scale; we ignore macroscopic sweep efficiency (influenced by rock heterogeneity and gravity over-run) which at field scale also impacts recovery.

The gw process, when gas displaces oil, is a primary drainage process, where the gas fills the largest available oil-filled throat. At the end of the displacement, gas will fill most of the larger pores, with water in the smaller ones and some remaining oil in pores of intermediate size.

In a spreading system – the spreading coefficient in Eq. (1) is zero, or close to zero – oil spreads as a layer in the pore space between gas and water. Gas never displaces water directly, as there is always a layer of oil in between [19]. In such cases, the oil remains connected throughout the pore space and very low residual oil saturations can be obtained (down to 1% or lower) for both secondary (gw process) and tertiary (wgw process, after waterflood) gas injection [11,12]. It is often considered that most reservoir systems, particularly if the gas and oil are nearly miscible, are spreading [57,58].

However, in this work, the fluid system we study is a highly non-spreading oil which disfavours the formation of layers. To quantify the impact, consider the Bartell-Osterhoff equation that places a constraint between the contact angles and the interfacial tensions [11].

$$\gamma_{gw} \cos \theta_{gw} = \gamma_{go} \cos \theta_{go} + \gamma_{ow} \cos \theta_{ow} \quad (3)$$

If we consider a strongly water-wet case, $\theta_{gw} = \theta_{ow} = 0$, then:

$$cos\theta_{go} = \frac{\gamma_{gw} - \gamma_{ow}}{\gamma_{go}} = 1 + S/\gamma_{go} \quad (4)$$

which, from Table 1, gives θ_{go} of around 50^o. This means that oil layers can only form in sharp corners of half-angle α less than 40^o ($\theta_{go}+\alpha<\pi/2$).

The significant amount of oil trapping is consistent with a non-spreading system. The oil can become disconnected during gas injection, as the oil does not surround the gas everywhere as a layer. This oil is trapped with gas during subsequent waterflooding through snap-off.

In a tertiary gas flood (wgw process, i.e. gas injection following a waterflood), layer flow allows the residual oil to reconnect, gas preferentially displaces oil and – as mentioned above – low residual oil saturations can be achieved. With a non-spreading oil, gas displaces both water and oil while oil remains poorly connected throughout the displacement. There is some displacement of oil but still the majority remains trapped after a further waterflood cycle.

During waterflooding, the gas is trapped principally by snap-off, where water invades the smallest regions of the pore space, disconnecting gas. The total amount of both oil and gas trapped for the gw sequence is larger than in a two-phase system.

For the wgw sequence, the residual gas saturation is exceptionally low – only 5%. In contrast, very little oil is displaced: Table 2 shows that the waterflood residual saturation is around 35% and the trapped oil saturation after further gas and water injection is over 29%. Indeed, the total amount of oil and gas trapped is almost exactly the two-phase residual. The gas will tend to rearrange the oil in the pore space through double drainage [21] so that it can occupy the larger pores. Some oil is displaced, and then water traps the gas in these larger pores, leading – overall – to a similar amount of trapping to that observed for the non-wetting phase in two-phase flow. The trapped gas clusters tend to span a single pore and are not as extensive as those seen after the gw sequence, as observed directly.

It should be noted that capillary end effects (which appear in water-wet plugs and which retain water at the outlet of the plug) may be significant in our study because of the small plug size; in field operations this effect can be neglected, and the residual saturations measured in our study may therefore not be representative of the true field-scale residual saturations. In addition we would like to stress that for CO_2-oil-water systems, a spreading coefficient close to zero (spreading situation) is expected [60], and this may change the fluid dynamics and/or thermodynamic fluid-fluid-fluid-solid pore-scale arrangement significantly.

Further work is required to study the effect of spreading coefficient, wettability and other displacement sequences on the behaviour and to establish what conditions are representative of reservoir displacements.

4. Conclusions

We have investigated the efficiency of two different three-phase flood sequences at the micrometre pore-scale level with micro-computed tomography in terms of their oil recovery and gas storage potentials. Our results demonstrate that significantly more oil can be produced by directly gas flooding a virgin oil reservoir (gw process, S_{or} = 21.6%) as compared to gas flooding a waterflooded oil reservoir (wgw process, S_{or} = 29.3%) under non-spreading conditions. In addition, our results indicate that much more gas can be stored using the gw process (S_{gr} = 20.6%; S_{gr} = 5.3% for the wgw process). These results have important implications for oil production and CCS schemes: a virgin oil reservoir would clearly be a better gas storage medium than a waterflooded one (neglecting other reservoir engineering factors such as injectivitiy/pressure-buildup or geo-mechanical effects). Furthermore, much more incremental oil can be produced if gas is directly injected into a virgin oil reservoir instead of following traditional waterflooding schemes.

We analysed the residual cluster size distributions and estimated the power-law exponents τ; τ was 2.02 and 2.03 for the three-phase residual oil cluster size distributions, which is similar to the τ estimated for an analogue two-phase (oil-brine) system (τ = 2.05; [37]). The gas clusters in the gw flood also had a similar τ (= 2.04)

associated, however the gas clusters in the wgw flood had a significantly different distribution exponent ($\tau = 2.32$). The results demonstrate that flooding history has a strong impact on fluid saturations and potentially cluster size distributions. Moreover, we found that residual gas clusters in the wgw flood were clearly much flatter than the gw gas clusters and the three-phase oil clusters (for both, the gw and wgw processes).

We also estimated the surface area/volume correlation exponent p for each system investigated, and find $p \approx 0.75$; this p is smaller than predicted by percolation theory ($p \approx 1$) with important implications for carbon geo-sequestration and contaminant transport, namely the residual phase dissolves more slowly in the aqueous phase because of reduced relative surface areas.

Acknowledgements

We would like to acknowledge our sponsor Shell under the Shell Grand Challenge on Clean Fossil Fuels and the Elettra Synchrotron Light Source Facility in Trieste, Italy, for providing beamtime and technical support.

References

[1] International Energy Agency. Key World Energy Statistics. Paris, 2010.

[2] Metz , B, Davidson, O, de Coninck, H, Loos, M, Meyer L (editors), Intergovernmental Panel on Climate Change Special Report on Carbon Dioxide Capture and Storage, Cambridge University Press, 2005.

[3] Lake, LW. Enhanced Oil Recovery, Richardson: SPE Publications; 2010.

[4] Iglauer, S, Wu, Y, Shuler, PJ, Tang, Y, Goddard, WA. New surfactant classes for enhanced oil recovery and their tertiary oil recovery potential. J Petrol Sci Eng 2010; 71: 23-29

[5] Iglauer, S, Wu, Y, Shuler, PJ, Tang, Y, Goddard, WA. Dilute iota- and kappa-Carrageenan solutions with high viscosity in high salinity brines. J Petrol Sci Eng; 75: 304-311.

[6] Firoozabadi, A, Cheng, P. Prospects for subsurface CO_2 sequestration. AIChE J 2010; 56: 1398-1405.

[7] Iglauer, S. Carbon capture and storage with a focus on capillary trapping as a mechanism to store carbon dioxide in geological porous media. In: Mewes D, Cheng L, editors. Advances in Multiphase Flow and Heat Transfer, Bussum: Bentham Science Publishers; 2012, p. 135-150.

[8] Qi, R, LaForce, TC, Blunt, MJ. A three-phase four-component streamline-based simulator to study carbon dioxide storage. Comput Geosci 2009; 13: 493-509.

[9] Skauge, A, Eleri, OO, Graue, A, Monstad, P. Influence of connate water on oil recovery by gravity drainage, Proc SPE Symp IOR 1994; SPE 27817.

[10] Kantzas, A, Chatzis, I, Dullien, FAL. Mechanisms of capillary displacement of residual oil by gravity-assisted inert gas injection. Proc SPE Reg Meet 1988; SPE 17506.

[11] Zhou, D, Blunt, MJ. Effect of spreading coefficient on the distribution of light non-aqueous phase liquid in the subsurface. J Contam Hydrol 1997; 25: 1-19.

[12] DiCarlo, DA., Sahni, A, Blunt, MJ. Three-phase relative permeability of water-wet, oil-wet, and mixed-wet sandpacks. SPE J 2000; 5: 82-91.

[13] Juanes, R, Spiteri, EJ, Orr, FM, Blunt, MJ. Impact of relative permeability hysteresis on geological CO_2 storage. Water Resour Res 2006; 42: W12418.

[14] Oak, MJ, Baker, LE, Thomas, DC. Three-phase relative permeability of Berea sandstone. J Petrol Technol 1990; 42:1054-1061.

[15] Shahverdi, H, Sohrabi, M, Fatemi, M, Jamiolahmady, M. Three-phase relative permeability and hysteresis effect during WAG process in miced wet and low IFT systems. J Petrol Sci Eng 2011; 78:732-739.

[16] Dumoré, JM, Schols, RS. Drainage capillary-pressure functions and the influence of connate water. SPE J 1997; 437-444.

[17] Keller, AA, Blunt, MJ, Roberts, PV. Micromodel observation of the role of oil layers in three-phase flow, Transport Porous Med 1997; 26: 277-297.

[18] Dong, M, Dullien, FAL, Chatzis, I. Imbibition of oil in film form over water present in edges of capillaries with an angular cross section. J Colloid Interf Sci 1995; 172:21-36.

[19] Chatzis, I, Kantzas, A, Dullien, FAL. On the investigation of gravity-assited inert gas injection using micromodels, long Berea sandstone cores and computer-assisted tomography, Proc SPE An Tech Conf 1988; SPE 18284.

[20] Oren, PE, Pinczewski, WV. Fluid distribution and pore-scale displacement mechanisms in drainage dominated three phase flow. Transport Porous Med 1995; 20: 105-133.

[21] Oren, PE., Billiote, J, Pinczewski, WV. Mobilization of waterflood residual oil by gas injection for water-wet conditions. SPE Form Eval 1992; 7: 70-78.

[22] Soll, WE, Celia, MA, Wilson, JL. Micromodel studies of three-fluid porous media systems: pore-scale processes relating to capillary pressure-saturation relationships. Water Resour Res 1993; 29: 2963-2974.

[23] Riazi, M, Sohrabi, M, Bernstone, Jamiolahmady, M, Ireland, S. Visualization of mechanisms involved in CO_2 injection and storage in hydrocarbon reservoirs and water-bearing aquifers. Chem Eng Res Des 2011; 89: 1827-1840.

[24] Stauffer, D. Scaling theory of percolation clusters. Phys Rep 1979; 54: 1-74.

[25] Al-Mansoori, SK, Iglauer, S, Pentland, CH, Blunt, MJ. Three-phase measurements of oil and gas trapping in sand packs. Adv Water Resour 2009; 32: 1535-1542.

[26] Egermann, P, Vizika, O, Dallet, L, Requin, C, Sonier, F. Hysteresis in three-phase flow: experiments, modelling and reservoir simulations. Proc SPE Euro Petrol Conf 2000; SPE 65127.

[27] Caubit, C, Bertin, H, Hamon, G. Three-phase flow in porous media: wettability effect on residual saturations during gravity drainage and tertiary waterflood. Proc SPE An Tech Conf 2004; SPE 90099.

[28] Iglauer, S, Wülling, W, Pentland, CH, Al-Mansoori, SK, Blunt, MJ. Capillary trapping capacities of consolidated rocks and sands. SPE J 2011; 16: 778-783.

[29] Pentland, CH, Tanino, Y, Iglauer, S, Blunt, MJ. Capillary trapping in water-wet sandstone: coreflooding experiments and pore-network modelling. SPE An Tech Conf 2010; SPE 133798.

[30] Iglauer, S, Fernø, M, Shearing, P, Blunt, MJ. Comparison of residual oil cluster size distribution, morphology and saturation in oil-wet and water-wet sandstone. J Colloid Int Sci 2012; 375, 187-192.

[31] Ortiz-Arango, JD, Kantzas, A. Visual study of the effect of viscosity ratio, flow rate and porous medium topology on two-phase relative permeabilities. Proc Can Int Petrol Conf; 2009.

[32] Lide, DR. CRC Handbook of Chemistry & Physics, Ohio: Chemical Rubber & Co; 2007.

[33] Morrow, N, Chatzis, I, Taber, J. Entrapment and mobilization of residual oil in bead packs. SPE Reservoir Engineering 1988; 3, 927-934.

[34] Münch, B, Trtik, P, Marone, F, Stampanoni, M. Stripe and ring artefact removal with combined wavelet – Fourier filtering, Opt Express 2009; 17: 8567-8591.

[35] Tschumperlé, D, Deriche, R. Vector-valued image regularization with PDE's: a common framework for different applications. Proc IEEE Comp Soc Conf Comp Vis Pat Recog 2003; 651-656.

[36] Otsu, N. A threshold selection method from gray-level histograms. IEEE Trans Syst Man Cyber 1979; 9: 62–66.

[37] Iglauer, S, Favretto, S, Spinelli, G, Schena, G, Blunt, MJ. X-ray tomography measurements of power-law cluster size distributions for the non-wetting phase in sandstones. Phys Rev E 2010; 82: 056315.

[38] Gittins, P, Iglauer, S, Pentland, CH, Al-Mansoori, SK, Al-Sayari, S, Bijeljic, B, Blunt, MJ. Nonwetting phase residual saturation in sand packs. J Porous Media 2010; 13:591-599..

[39] Al-Mansoori, SK, Itsekiri, E, Iglauer, S, Pentland, CH, Bijeljic, B, Blunt, MJ. Measurements of non-wetting phase trapping applied to carbon dioxide storage, Int J Greenh Gas Con 2010; 4: 283-288.

[40] Pentland, CH, Itsekiri, E, Al-Mansoori, SK, Iglauer, S, Bijeljic, B, Blunt, MJ. Measurement of nonwetting-phase trapping in sandpacks. SPE J 2010; 15:27-277.

[41] Fayers, FJ. Extension of Stone's method 1 and conditions for real characteristics in three-phase flow. SPE Res Eng 1987; 4:437-445.

[42] Dias, MM, Wilkinson, D. Percolation with trapping. J Phys A 1986; 19: 3131-3146.

[43] Blunt, MJ, Scher, H. Pore-level modelling of wetting. Phys Rev E 1995; 52: 6387-6403.

[44] Lorenz, CD, Ziff, RM. Precise determination of the bond percolation thresholds and finite-size scaling corrections for the sc, fcc, and bcc lattices. Phys Rev E 1998; 57: 230-236.

[45] Landry, CJ, Karpyn, ZT, Piri, M. Pore-scale analysis of trapped immiscible fluid structures and fluid interfacial areas in oil-wet and water-wet bead packs. Geofluids 2011; 11: 209-227.

[46] Iglauer, S, Paluszny, A, Pentland, CH, Blunt, MJ. Residual CO_2 imaged with x-ray micro-tomography. Geophys Res Lett 2011; 38:L21403.

[47] Pentland, CH, El-Maghraby, R, Iglauer, S, Blunt, MJ. Measurements of the capillary trapping of super-critical carbon dioxide in Berea Sandstone. Geophys Res Lett 2011; 38:L06401.

[48] Plug, WJ, Bruining, J. capillary pressure for the sand-CO_2-water system under various pressure conditions. Application to CO_2 sequestration. Adv Water Resour 2007; 30:2339-2353.

[49] Berg, S, Oedai, S, Ott, H. Displacement and mass transfer between saturated and unsaturated CO_2-brine systems in sandstone. Int J Greenh Gas Con 2012; in press.

[50] Chalbaud, C., Robin, M., Mombard, J.-M., Bertin, H., Egeremann, P. Oil & Gas Science and Technology 2010; 65:541-555.

[51] Bikkina, PK. Contact angle measurements of CO_2-water-quartz/calcite systems in the perspective of carbon sequestration. Int. J. Greenh. Gas Con. 2011; 5: 1259-1271.

[52] Chiquet, P, Broseta, D, Thibeau, S. Wettability alteration of caprock minerals by carbon dioxide. Geofluids 2007; 7:112-122.

[53] Espinoza, DN, Santamarina, JC. Water-CO_2-mineral systems: Interfacial tension, contact angle, and diffusion – Implications to CO_2 geological storage. Water Resour Res 2010; 46: W0753.

[54] Yang, D, Gu, Y, Tontiwachwuthikul, P. Wettability determination of the reservoir brine-reservoir rock system with dissolution of CO_2 at high pressures and elevated temperatures. Energ Fuel 2008; 22:504-509.

[55] Liu, SY, Yang, XN, Qin, Y. Molecular dynamics simulation of wetting behaviour at CO_2/water/solid interfaces. Chinese Sci Bull 2010; 55:2252-2257.

[56] Iglauer, S, Mathew, M, Bresme, F. Molecular dynamics computations of brine-CO_2 interfacial tensions and brine-CO_2-quartz contact angles and their effects on structural and residual trapping mechanisms in carbon geo-sequestration", J Colloid Int Sci, in press.

[57] Iglauer, S. Dissolution Trapping of Carbon Dioxide in Reservoir Formation Brine – A Carbon Storage Mechanism. In: Nakajima, H, editor. Mass Transfer - Advanced Aspects, Rijeka: InTech; 2011.

[58] Israelachvili, JN. Intermolecular and surface forces. Amsterdam: Academic Press; 2011.

[59] Kantzas, A, Chatzis, I, Dullien, FAL. Enhanced oil recovery by inert gas injection. Proc SPE Enhanc Oil Recov Symp 1988; SPE 17379.

[60] Melean, Y, Bureau, N, Broseta, D. Interfacial effects in gas-condensate recovery and gas-injection processes. SPE Res Eval Eng 2003; 6:244-254.